International Journal of Mechanical, Industrial and Aerospace Sciences
ISSN: 2517-9950
Vol:14, No:3, 2020

Flame Kernel Growth and Related Effects of Spark Plug Electrodes: Fluid Motion Interaction in an Optically Accessible DISI Engine

A. Schirru, A. Irimescu, S. Merola, A. d'Adamo, S. Fontanesi

***Abstract*—**One of the aspects that are usually neglected during the design phase of an engine is the effect of the spark plug on the flow field inside the combustion chamber. Because of the difficulties in the experimental investigation of the mutual interaction between flow alteration and early flame kernel convection effect inside the engine combustion chamber, CFD-3D simulation is usually exploited in such cases. Experimentally speaking, a particular type of engine has to be used in order to directly observe the flame propagation process. In this study, a double electrode spark plug was fitted into an optically accessible engine and a high-speed camera was used to capture the initial stages of the combustion process. Both the arc and the kernel phases were observed. Then, a morphologic analysis was carried out and the position of the center of mass of the flame, relative to the spark plug position, was calculated. The crossflow orientation was chosen for the spark plug and the kernel growth process was observed for different air-fuel ratios. It was observed that during a normal cycle the flow field between the electrodes tends to transport the arc deforming it. Because of that, the kernel growth phase takes place away from the electrodes and the flame propagates with a preferential direction dictated by the flow field.

***Keywords*—**Combustion, Kernel growth, optically accessible engine, spark-ignition engine, spark plug orientation.

I. Introduction

IN an era where the world is fighting a climate crisis due to greenhouse gases emissions, the transportation field is asked to improve its efficiency [1]. That task is particularly hard for car manufacturers that have to respect stricter limitations year after year on exhaust emissions of their vehicles. In this scenario, internal combustion engines need to be drastically improved with new designs and combustion's techniques. As the spark-ignited engines seem to be more suitable for this "mission", new combustion concepts have to be developed. One of these is the "ultra-lean" combustion which allows reducing the temperatures inside the combustion chamber and the NOx emissions as a consequence [2], [3]. Working with such lean mixtures and low temperatures also has its problems. Usually, it became hard to ignite the air-fuel mixture and so it was necessary to generate a stratified charge with a richer mixture in the proximity of the spark plug. With this aim, GDI (Gasoline Direct Injection) systems were developed, where an injector inside the combustion chamber is employed to achieve such stratification.

Another problem with ultra-lean combustion is the high value of cyclic variability. Cycle-to-cycle variability (CCV) is ultimately caused by the turbulent nature of the in-cylinder flow field [4], [5]. Given that combustion in ultra-lean condition is slower than usual, the effect of the turbulence is emphasized, and it can result in an excessive irregularity that can lead to reduced thermal efficiency, increased pollutant emission (e.g. incomplete combustion), and high fuel consumption [6]. As discovered by Schiffmann et al. [7], the very first stages of the combustion process have an extreme importance over the whole combustion event. That being said, increasing attention is needed during this phase.

In particular, what triggers the combustion process in GDI engines is the spark plug. At first, its geometry has been extensively studied by many authors but recently, more attention was drawn to its orientation [8]. The effect of this parameter has been first analyzed from a numerical point of view exploiting CFD-3D simulations [9]. These types of analyses have the advantage to be fast, easily repeatable and low cost compared to experiments. On the other hand, the ignition process is characterized by time and spatial scales much smaller than the ones usually resolved in that type of simulations; as a result, the grid size and the time-step must be massively reduced, inevitably increasing computational efforts. Therefore, ignition models, with the ability to reproduce the effect of this phase without directly resolving it, must be developed.

To render an ignition model robust enough to be reliable in many different operative conditions, a database of experimental results is needed in order to have a successful validation. While in traditional engines it is impossible to observe the combustion process evolution, it can be done in optically accessible ones. Wang et al. [10] used an optically accessible engine to see the effect of the orientation of the spark plug. In their work, the kernel growth was observed from a plane parallel to the spark plug axis. They have shown that the kernel is transported by tumble motion and that the flame propagates in the same direction. It was also found that there is not a simple correlation between the spark plug's orientation and kernel growth rate. That type of inconsistency in the results could also be the reason why Aleiferis et al. [11] and Anderson [12] found different spark plug orientation as optimal to reduce CCV.

Andrea Schirru, Alessandro d'Adamo and Stefano Fontanesi are with the University of Modena and ReggioEmilia, Via Vivarelli 10, 41122 Modena, Italy (e-mail: alessandro.dadamo@unimore.it; stefano.fontanesi@unimore.it; schirru.andrea@alice.it).

*Adrian Irimescu and Simona Merola are with CNR–Istituto Motori, via G. Marconi 4, 80125 Napoli, Italy (*corresponding author, e-mail: s.merola@im.cnr.it; *a.irimescu@im.cnr.it).

In this work, a double-electrode spark plug was fitted into an optically accessible GDI spark ignition (SI) engine. Both thermodynamic and optical analyses were carried out focusing on the first stages of the combustion process. Three different values of dilution ratio λ with three different spark timing were analyzed to see the effect that turbulence (and related interactions with the spark plug electrodes) has on flame propagation. A symmetric spark plug orientation with the electrodes perpendicular to the direction of tumble (crossflow configuration, achieved by placing an additional washer below the plug) was chosen to create a database suitable for ignition model validation in a CFD-3D environment. In a second stage, the default spark plug orientation was considered (by removing the additional washer) to observe the differences from the previous one.

II. Experimental Setup

A. Engine

Measurements were performed on an optically accessible direct injection spark ignition (DISI) engine; a mass-produced 4 valves per cylinder head from a 1.4 litres Fiat 4-cylinder engine is coupled to the base by a custom flange. The base features a Bowditch design [13] to allow the combustion chamber to be visible through the piston crown (Fig. 1). The main parameters regarding the engine are collected in Table I (with CAD for crank angle degrees, "b" for before and "a" for after top dead centre TDC); it featured centrally located spark plug and side-mounted injector for wall-guided operation. Injection pressure was maintained at 100 bar. All cases were studied at wide open throttle (WOT) conditions; the air-fuel ratio was measured using a wide-band exhaust gas oxygen sensor, with an accuracy of ± 1%. The engine was operated in naturally aspirated mode with the air temperature inside the test cell around 290 K.

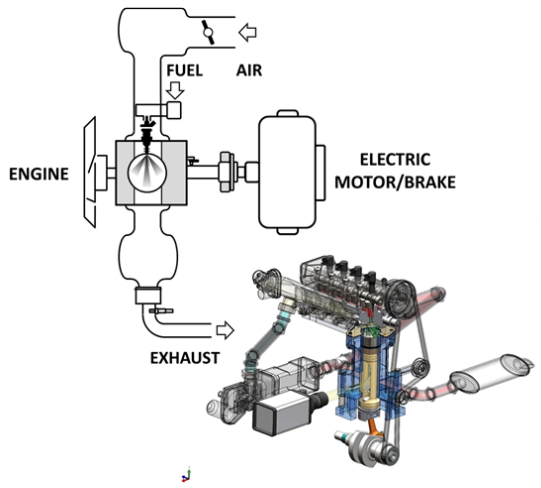

Fig. 1 Schematic representation of the experimental setup and illustration of the optical accessibility through the piston via a UV-enhanced mirror tilted at 45 degrees [14]

Operating conditions are listed in Table II. The start of injection was the same for all conditions and the relative air-fuel ratio (λ) value was varied by modifying the duration of injection (DOI). The spark advance (SA) was set so that the crank angle at which there is a mass fraction burnt MFB of 50% (MFB50), was around 15 CAD aTDC. This was found to be a good compromise of ignition close to the point of maximum brake torque (MBT) as well as ensuring stable operation in a wide range of air-fuel ratios.

TABLE I
Engine Specifications

Displacement	399 cm^3
Stroke	81.3 mm
Bore	79 mm
Connecting Rod	143 mm
Compression Ratio	10:1
Number of Valves	4
Exhaust Valves Open	153 CAD aTDC
Exhaust Valves Close	360 CAD aTDC
Intake Valves Open	363 CAD bTDC
Intake Valves Close	144 CAD bTDC

TABLE II
Operative Conditions

Rotation Speed	λ	SA [CAD]	DOI [CAD]
1000rpm	1.0	08	23
	1.1	10	21
	1.2	12	19.2

It was chosen to employ a double electrode spark plug so it was possible to provide a complete view of the kernel right from its inception while ensuring performance levels comparable to those obtained with a 'classical' J-type ground electrode design [6]. A piezo-resistive transducer was used to measure the in-cylinder pressure with an accuracy of ± 1% and with a resolution of 0.2 CAD. A simplified heat release analysis, with constant ratio of specific heats [14], was performed for calculating combustion phasing parameters and volume fraction burned (VFB) traces.

B. Optical Setup

Early flame front propagation was investigated through cycle resolved digital imaging. Visualization was performed with a high-speed CMOS camera (CamRecord 5000, 8-bit, 16 µm x 16 µm pixel size by Optronis, Kehl, Germany) equipped with a 50 mm Nikon objective. The camera worked in full chip configuration (512 x 512 pixel) acquiring 5000 frames per second with an exposure time of 167 µs. An aperture of f/2.8 was set to improve the signal-to-noise ratio without extensive saturation effects. Therefore, the set-up allowed the images to be recorded with a dwell time of 1.2 CAD at 1000 rpm and a spatial resolution of 0.18 mm per pixel. The optical acquisition for each operative condition consisted of 40 frames per cycle after spark timing, during 100 consecutive engine cycles.

A consolidated image processing procedure allowed the evaluation of macroscopic parameters related to flame morphology by applying a routine developed in Vision of National Instruments; details are reported in [15]-[17]. First of all, a mask was created for the images of each sequence to

identify the limit of the optical window (Fig. 2 (a)). Then a lookup table was used to modify contrast and brightness so that the flame boundaries were more defined (Fig. 2 (b)). Later, the image was binarized choosing various threshold settings for different λ values (from 15 for λ = 1.2, to 22 for the stoichiometric condition) (Fig. 2 (c)). In the end, a fast Fourier transform (FFT) filter is used to reduce the noise level in the binarized image (Fig. 2 (d)).

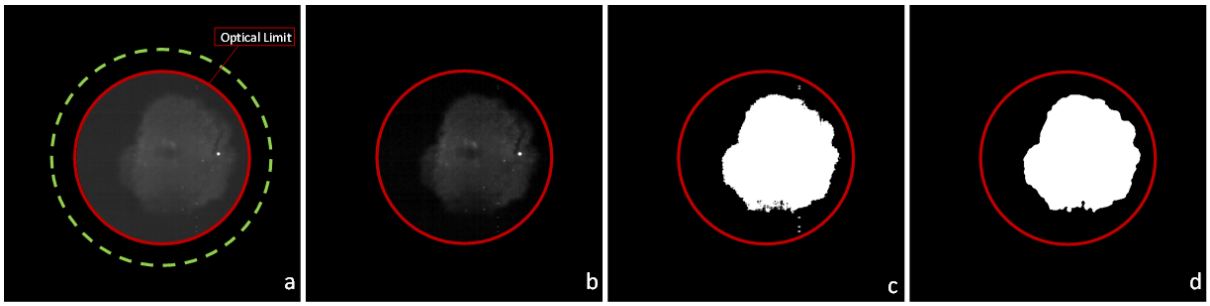

Fig. 2 Image processing procedure: (a) Mask, (b) Lookup Table, (c) Binarization, (d) FFT Filter

Advanced morphology functions applied to the binary images allowed the estimation of several flame parameters such as area, centre of mass position (CM) and Heywood circularity factor (HCF).

Flame area (A) corresponded to the number of pixels included in the foreground of binary images. For our analysis, a coordinate system with the origin coincident with the spark plug axis has been used to define the position of the flame center of mass. Finally, HCF is defined as the ratio between the perimeter of the binarized image and the circumference of a circle with the same area. This parameter is an index of how deformed the flame front is.

III. Data Analysis

Once the image processing has been completed for each operative condition, the next step is to couple thermodynamic and optical data. That process is done thanks to a script developed in LabView of National Instrument.

The MFB trace is calculated for all the optically acquired cycles using a simplified heat release rate analysis [14]. In that way, it is possible to obtain a coupling between crank angle (CA) and MFB. The next thing to do is to assign a CA to a certain image. To do that, the trigger signal of the camera is used. The signal can be divided into three main phases: rising edge, falling edge and a constant phase. This last phase corresponds to the period of time the camera chip is exposed to the light, so the final image will be a representation of all the different positions of the flame in such a time. During the image processing phase, all the optical data extracted from an image are relative to the moment in which the flame is larger during the exposure time. For this reason, the start of the falling edge (end of the exposure time) is considered to be more representative of the moment captured in a particular frame. Having finished this phase, it is now possible to have a good match between thermodynamic and optical data.

The next step is to select the images corresponding to the arc and kernel phase. For the first ones, there was more than one frame showing the arc for each cycle, so a CA-based filter was used to select only one image per cycle. In particular, the second image for each acquired cycle was chosen. To observe the kernel phase, images corresponding to MFB equal to 5% (MFB5), were selected. Because of the low accuracy of the method used to calculate MFB when its value is lower than 10%, an area-based filter was used. This method is based on the assumption that there is a linear correlation between volume fraction burnt (VFB) and the flame area (Fig. 3). Please note that the "Area" on the ordinate axis has been normalized to the piston cross-section.

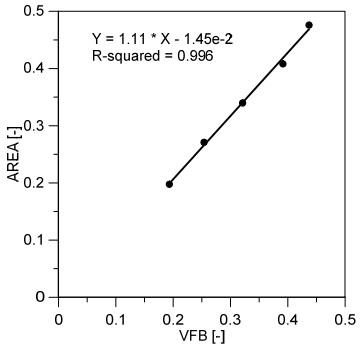

Fig. 3 VFB vs Area, for the operative condition with λ = 1.1

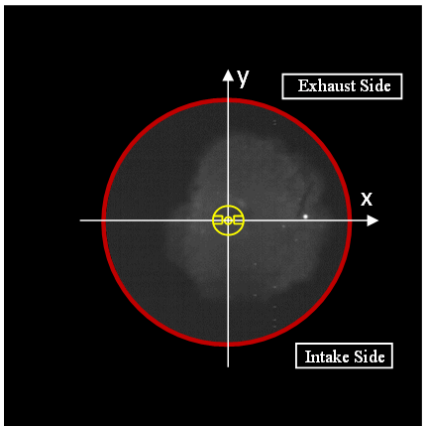

Fig. 4 Conventional coordinate system

Given that VFB is defined by (1), it is obvious that there is a direct correlation between MFB and VFB [18]:

$$VFB = \left[1 + \frac{1-MFB}{\left(\rho_u/\rho_b\right)MFB}\right]^{-1}, \quad (1)$$

where ρ indicates the density of the unburnt (subscript "u") and burnt (subscript "b") mixture. The ratio between these two densities was assumed around 4 [18]. That being said, an average area for the images corresponding to MFB10 has been calculated so that the half of such area can be used as a filter to select the images corresponding to MFB5. In particular, an area of about 18000 pixels was found to be the one corresponding to MFB5 and an interval of ± 1000 pixels was used as a range around that area to select the right images.

The last thing to do is the transformation of the value from pixel to mm (for distances/lengths), and mm^2 for surfaces. For practical reasons the coordinates of the flame center of mass are transferred to a coordinate system with the origin centered on the spark plug axis (Fig. 4).

IV. Results

In this section, the results extracted from both the thermodynamic and optical analysis will be presented. In particular, in the first part, a brief thermodynamic analysis will be carried out, followed by the presentation of the results from the optical analysis and in the end the comparison between the two different spark plug orientations will be shown.

A. Thermodynamic Results

In Fig. 5, the mean pressure traces regarding the three operative conditions with different λ values and spark timing settings are presented. As expected, the higher λ, the lower the maximum pressure is.

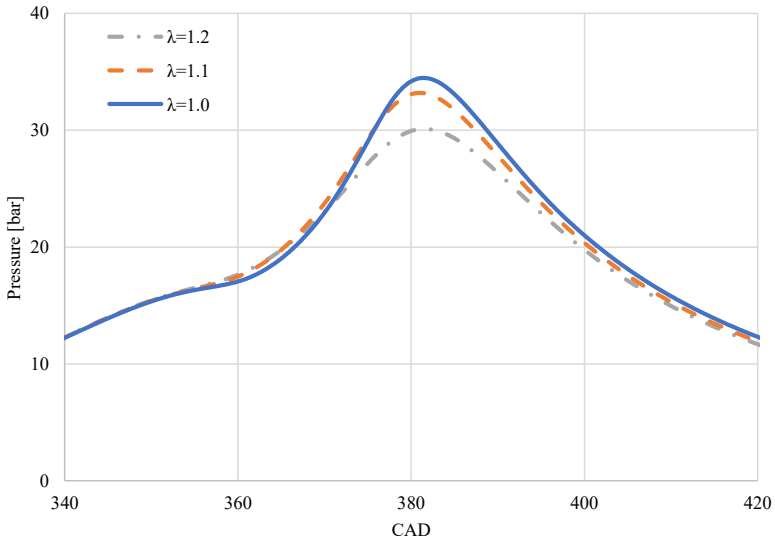

Fig. 5 In-cylinder pressure traces for the three conditions

An overview of engine performance can already be inferred from Fig. 5, with clear comparison shown in Fig. 6 (a). In fact, the conditions with lower λ values, that had a lower peak pressure than the richer ones, also have lower indicated mean effective pressure (IMEP) values. This result is derived from an average of 200 IMEP values for each operative condition, so it does not give any information on combustion stability. In Fig. 6 (b), the coefficient of variation (COV) of the IMEP is presented. As usual, having a slower combustion gives the turbulence a longer time to affect the flame propagation and so a larger COV is expected. That is confirmed in Fig. 6 (b), where it is possible to observe a trend where leaner conditions have higher COVs.

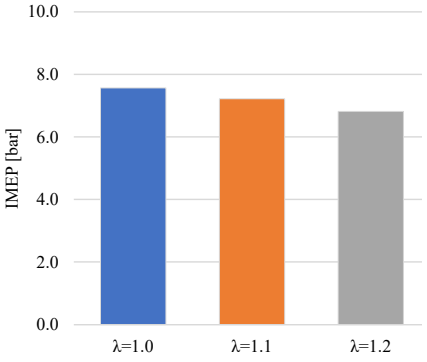

Fig. 6 (a) Average IMEP

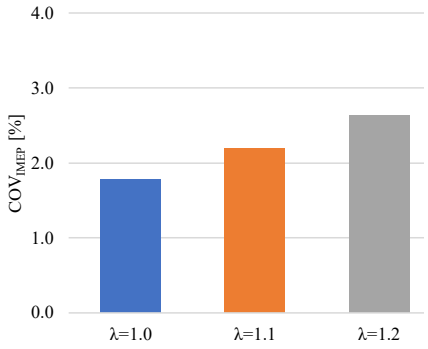

Fig. 6 (b) COV for the IMEP

B. Optical Results

Following the analysis of optical results, spark arc and flame propagation were the main areas of interest. A representative sequence of stoichiometric combustion is shown in Fig. 7. The images were chosen to illustrate how the flame propagated from spark timing to the moment it reaches the optical limit (and could no longer be visualized through the piston crown).

The images proposed in Fig. 7 are in chronological order from left to right. It can be noticed that the arc was formed on the right hand side electrode and the flame features preferentially propagation in the same direction. Moreover, the flow field in the combustion chamber seems to influence this direction by pushing the flame from the intake to the exhaust side. That type of interaction can be found on the majority of the acquired sequences suggesting the presence of tumble motion.

The images in Fig. 8, are referred to the two extreme conditions $\lambda = 1.0$ and $\lambda = 1.2$. The first noticeable thing is the difference in brightness between the two. The stoichiometric one is brighter (as expected) meaning that a larger amount of energy has been released (so higher concentration of active species is likely to be present) in comparison to the leaner condition. Then, some considerations on CCV can be done. While in the stoichiometric condition, the flame propagates in an almost circular way, the second condition has a much more distorted shape. That may be due to the longer time that the turbulence has influenced the flame front from spark timing to the captured moment. Moreover, the direction in which the flame propagates seems to be much more variable than in the first condition.

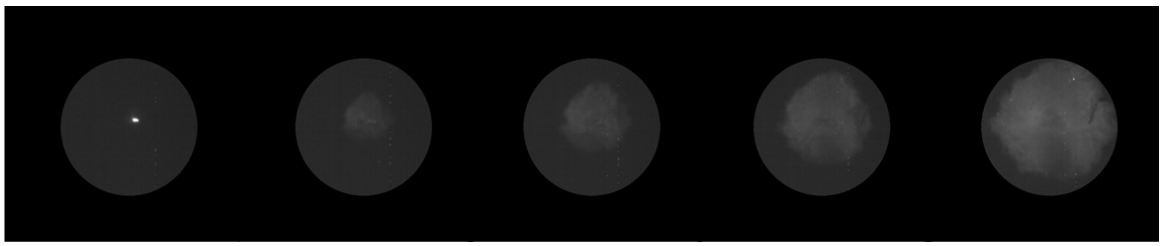

Fig 7 Representative sequence of the flame propagation process for the stoichiometric condition

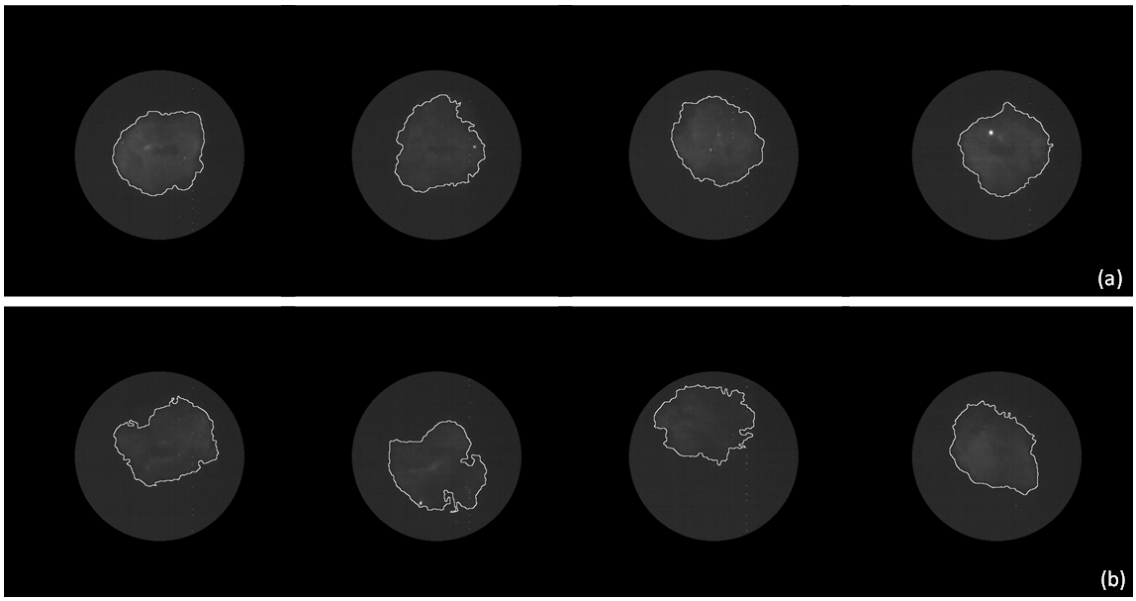

Fig. 8 Four images corresponding to MFB5 are presented for two conditions: (a) $\lambda = 1.0$; (b) $\lambda = 1.2$; a perimeter line is superimposed to improve the image visibility

The marked differences between the images in Fig. 8 (b) result in greater COV for the leaner condition, confirming the trend shown before in Fig. 6 (b). That being said, a more global analysis will now be carried out to observe the way in which an average cycle for a certain operative condition would behave. At this stage, both the arc and the kernel phase will be considered.

While analyzing the results, it is important to keep in mind that the arc deformation along direction "y" is mostly due to the flow field direction with respect to the electrodes (i.e. organized tumble motion and turbulence); along "x" it's a more complex phenomenon, with an additional degree of freedom. Given that the spark plug features two ground J-type electrodes, symmetric with respect to the "y" axis, the CM position along "x" gives an indication on which side has the higher probability to create a spark. It is important to remember that the spark is generated along the lowest resistance path and so local temperatures, micro-turbulence and local mixture composition play a key role in the result.

Observing the graph regarding CM Y, for both arc and kernel phase, a trend can be noted, where for operative conditions with leaner mixtures, both the arc and the kernel tend to propagate towards the exhaust side supporting the hypothesis that tumble motion persisted during the combustion phase. While looking at the arc results it must also be considered that, for the three different λ values, three different SA have been used. So, the slight differences in CM Y for the arc phase of the considered operative conditions are probably the result of different tumble and turbulence intensities for each spark timing. That's coherent with what is normally observed; in fact, leaner conditions are more conditioned by tumble, having the greater SA and that same effect has an impact of the rest of the combustion process.

It is important to note that, having considered the flame center of mass, the asymmetry in flame propagation is less visible compared to the situation of showing the extreme points reached by the flame. Moreover, comparing the dimensions of the electrodes summarized in Fig. 10, and the values presented in Fig. 9, it can be seen that the CM is always between the electrodes, except for the condition with λ = 1.2 where the most probable kernel CM position is just 0.6 mm far from the electrodes along the "y" direction.

Moving to graphs in Figs. 9 (c) and (f), the decision to consider the perimeter as a parameter of the arc deformation comes from the consideration that compared to the kernel, the arc has an almost linear shape and so the HCF would not be a suitable parameter.

It can be observed that the differences between the different operative conditions are almost negligible in terms of arc perimeter, in fact, a difference of less than 3% is found between the two extreme conditions. Such contained difference is probably caused by lower turbulence intensity in the combustion chamber because of the reduced rotational speed.

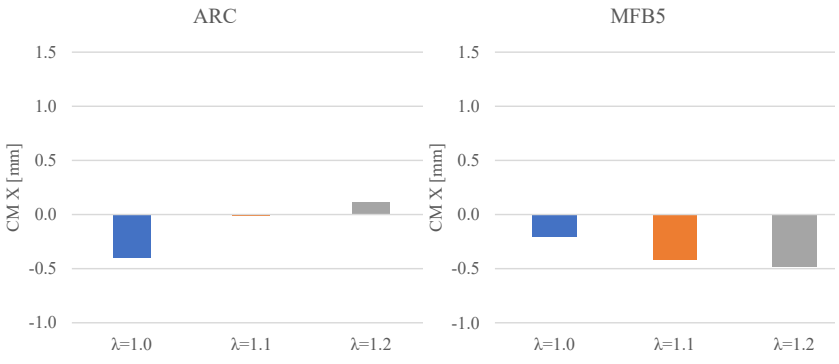

(a) (d)

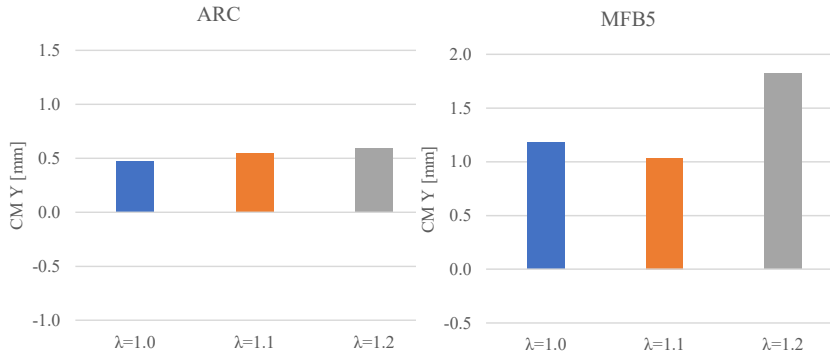

(b) (e)

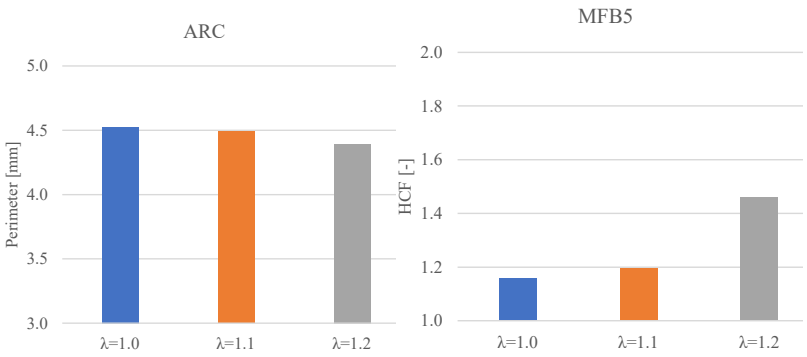

Fig. 9 Average optical results, for the arc phase (a), (b), (c) and flame kernel (d), (e), (f)

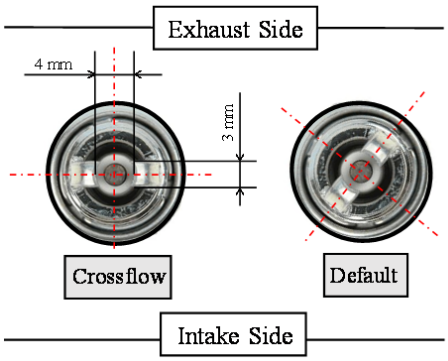

Fig. 10 Geometrical properties of the double J-type electrode spark plug

C. Spark Plug Orientation

In this section, a comparison between two spark plug orientations (i.e. the previous situation with crossflow configuration, compared to the default condition, with the additional washer removed) is proposed. The two configurations have been called "A" (designated as "Crossflow" in Fig. 10) and "B" (identified as "Default" in Fig. 10). The first one is the crossflow configuration and the second one is the default configuration with the electrode's direction rotated by around 50 degrees. The default orientation is conditioned by the way the treading is done inside the engine's head and on the spark plug while the orientation was modified to obtain the crossflow's one by adding a washer (width = 1.3 mm), to the spark plug.

Fig. 11 shows the position of the center of mass, expressed according to a polar coordinate system centered in the spark plug axis. Distance (Fig. 11 (a)), and direction (Fig. 11 (b)), were both analyzed.

Starting with the distance, the observed trend for configuration A is confirmed in the second one. In fact, for both configurations, the average flame center of mass is further from the spark plug for leaner conditions. Moreover, the electrodes' orientation also seems to affect the local flow field. One hypothesis is that in configuration B the electrodes behave like a barrier from the flow field resulting in lower flame transportation.

For the direction in which the flame is deformed, given that the tumble direction is assumed to be at 90 degrees, it can be seen that the flames tend to propagate towards a direction around 65 degrees for all configurations, suggesting a combined effect of the tumble and another air flow inside the combustion chamber. The reason for this additional ordered fluid motion is unclear (i.e. the four valves configuration should result in tumble and practically zero swirl). One possible explanation is that the operative cylinder is coupled with mass produced head derived by a four-cylinder engine, so the temperature distribution on the cylinder liner might not be uniform. Anyway, while a trend with λ can still be observed, the influence of the spark plug orientation seems to be less important. Please notice that while considering these operative conditions with different λ values, the difference in the spark timing can be the dominant motivation of such trends.

The effect different configurations have on the engine performance can be observed in Fig. 12. While the same trend is maintained varying λ for both the spark plug orientations, a small difference for both the IMEP and COV values has been observed. In fact, slightly lower IMEP value together with a higher COV (Figs. 12 (a) and (b) respectively), was found for the crossflow configuration in comparison with the default one. More in detailed analysis, exploiting both CFD and experimental tools will be needed to explain such trends.

V. Conclusions and Further Developments

During this work, a DISI optically accessible engine, fitted with a double J-type ground electrode spark plug has been exploited to investigate the effect of different λ values and spark timing on flame front propagation. Optical and thermodynamic analyses have been carried out and the results were presented in two main sections. The effect of tumble motion was observed as both the kernel and the arc tend to deform preferentially towards the exhaust side; only small asymmetries were observed because of the reduced turbulence levels. These are correlated with the chosen rotational speed (1000 rpm), which does not seem to be high enough to generate a strong turbulent flow field. Then, the effect of the spark plug orientation was discussed and it was observed that while it may have a considerable effect on the distance at

which the center of mass is translated by the flow field, it does not seem to be so relevant with respect to the direction in which the flame is propagating.

As for future developments in this field, the same analysis will be carried out for higher rotational speeds to observe the different effect higher turbulence intensity has on flame propagation. Moreover, other spark plug's orientations will be tested such as "the parallel flow", so that the influence the electrodes have on the local flow field will be deeply investigated.

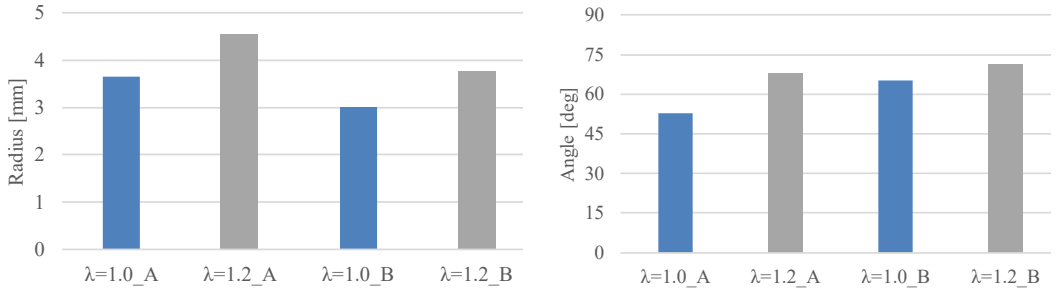

(a) (b)

Fig. 11 Comparison between two spark plug orientations in terms of (a) distance from the spark plug axis and (b) direction in which the center of mass has been transported

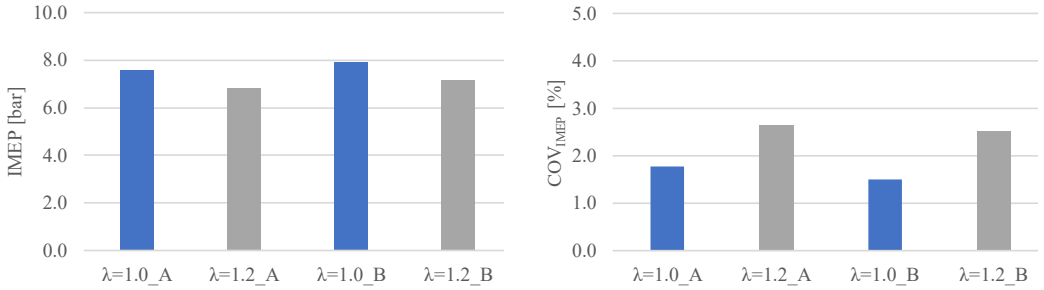

(a) (b)

Fig. 12 Thermodynamic comparison between two spark plug orientations

REFERENCES

[1] Communication from the Commission to the European Parliament, the European Council, the Council, the European Economic and Social Committee, the Committee of the Regions and the European Investment Bank. A Clean Planet for all A European strategic long-term vision for a prosperous, modern, competitive and climate neutral economy COM/2018/773 final.

[2] Ferrari, Giancarlo Internal Combustion Engines, Società Editoriale Esculapio, 2016, pp. 471-519.

[3] Cimarello, A. (a.a. 2014-2015). Analysis of Advanced Ignition Systems in Leaning Operating Conditions using an Optical Access Engine. Tesi di dottorato. Università degli Studi di Perugia, Dipartimento di Ingegneria.

[4] Ozdor, N., Dulger, M., and Sher, E., "Cyclic Variability in Spark Ignition Engines: A Literature Survey," SAE Technical Paper 940987, 1994, 10.4271/940987.

[5] Fontanesi, S., d'Adamo, A., Rutland, C.J., "Large-Eddy simulation analysis of spark configuration effect on cycle-to-cycle variability of combustion and knock", International Journal of Engine Research, 2015, doi:10.1177/1468087414566253.

[6] d'Adamo, Alessandro & Breda, Sebastiano & Berni, Fabio & Fontanesi, Stefano. (2018). Understanding the Origin of Cycle-to-Cycle Variation Using Large-Eddy Simulation: Similarities and Differences between a Homogeneous Low-Revving Speed Research Engine and a Production DI Turbocharged Engine. SAE International Journal of Engines. 12. 10.4271/03-12-01-0007.

[7] Schiffmann, P., "Root Causes of Cycle-To-Cycle Combustion Variations in Spark Ignited Engines," Ph.D. thesis, University of Michigan, Ann Arbor, MI, USA, 2016.

[8] Ge, Haiwen & Zhao, Peng. (2019). Numerical Investigation of the Spark Plug Orientation Effects on Flame Kernel Growth. 10.4271/2019-01-0005.

[9] Shekhawat, Yajuvendra & Haworth, D.C. & d'Adamo, Alessandro & Berni, F. & Fontanesi, Stefano & Schiffmann, Philipp & Reuss, David & Sick, V.. (2017). An Experimental and Simulation Study of Early Flame Development in a Homogeneous-charge Spark-Ignition Engine. Oil and Gas Science and Technology. 72. 10.2516/ogst/2017028.

[10] Wang, Yanyu, et al. "Investigation of Impacts of Spark Plug Orientation on Early Flame Development and Combustion in a DI Optical Engine." SAE International Journal of Engines, vol. 10, no. 3, 2017, pp. 995–1010. JSTOR, www.jstor.org/stable/26285106. Accessed 27 Jan. 2020.

[11] Aleiferis, P., Taylor, A., Whitelaw, J., Ishii, K. et al., "Cyclic Variations of Initial Flame Kernel Growth in a Honda VTEC-E Lean-Burn Spark-Ignition Engine," SAE Technical Paper 2000-01-1207, 2000, https://doi.org/10.4271/2000-01-1207.

[12] Anderson, R. W., and J. R. Asik. "Ignitability Experiments in a Fast Burn, Lean Burn Engine." SAE Transactions, vol. 92, 1983, pp. 390–404. JSTOR, www.jstor.org/stable/44668078. Accessed 27 Jan. 2020.

[13] Bowditch, F., "A New Tool for Combustion Research A Quartz Piston Engine," SAE Technical Paper 610002, 1961, doi:10.4271/610002.

[14] Irimescu, A., Merola, S., and Martinez, S., "Influence of Engine Speed and Injection Phasing on Lean Combustion for Different Dilution Rates in an Optically Accessible Wall-Guided Spark Ignition Engine," SAE Int. J. Engines 11(6):1343-1369, 2018, https://doi.org/10.4271/2018-01-1421.

[15] Merola, S.S., Marchitto, L., Tornatore, C., Valentino, G., and Irimescu, A., "Optical Characterization of Combustion Processes in a DISI Engine Equipped with Plasma-Assisted Ignition System," Appl. Therm. Eng. 69(1-2):177-187, 2014, doi:10.1016/j.applthermaleng.2014.04.046.

[16] Irimescu, A.; Marchitto, L.; Merola, S.S.; Tornatore, C.; Valentino, G. Evaluation of different methods for combined thermodynamic and optical analysis of combustion in spark ignition engines. Energy onvers. Manag. 2014, 87, 914–927, doi:10.1016/j.enconman.2014.07.037.
[17] Martinez, S.; Irimescu, A.; Merola, S.; Lacava, P.; Curto, P. Flame Front Propagation in an Optical GDI Engine under Stoichiometric and Lean Burn Conditions. Energies 2017, 10, 1337, doi:10.3390/en10091337.
[18] Heywood, John B. Internal Combustion Engine Fundamentals. New York: McGraw-Hill, 1988, pp. 392.